

OPEN ACCESS

EDITED BY Stefania Fiorcari, Azienda Ospedaliero Universitaria di Modena, Italy

REVIEWED BY
Prapansak Srisapoome,
Kasetsart University, Thailand
Liangwen Chen,
Wuhan University, China
Adili Alimujiang,
Jinan University, China

RECEIVED 20 June 2025 ACCEPTED 29 September 2025 PUBLISHED 20 October 2025

CITATION

Zhao R, Wang L, Zhou Y, Xiao K, Liu Q and Yu K (2025) LncRNA NRIR inhibits osteogenesis by promoting macrophage M1 polarization through RSAD2/NF-κB axis in peri-implantitis. *Front. Immunol.* 16:1650984. doi: 10.3389/fimmu.2025.1650984

COPYRIGHT

© 2025 Zhao, Wang, Zhou, Xiao, Liu and Yu. This is an open-access article distributed under the terms of the Creative Commons Attribution License (CC BY). The use, distribution or reproduction in other forums is permitted, provided the original author(s) and the copyright owner(s) are credited and that the original publication in this journal is cited, in accordance with accepted academic practice. No use, distribution or reproduction is permitted which does not comply with these terms.

LncRNA NRIR inhibits osteogenesis by promoting macrophage M1 polarization through RSAD2/NF-kB axis in peri-implantitis

Renshengjie Zhao^{1,2,3}, Lan Wang^{1,2,3}, Yang Zhou^{1,2,3}, Keming Xiao^{1,2,3}, Qiqi Liu^{1,2,3} and Ke Yu^{1,2,3}*

¹The Affiliated Stomatological Hospital, Southwest Medical University, Luzhou, China, ²Oral & Maxillofacial Reconstruction and Regeneration of Luzhou Key Laborator, Luzhou, China, ³Institute of Stomatology, Southwest Medical University, Luzhou, China

Introduction: Peri-implantitis is an inflammatory condition affecting the hard and soft tissues surrounding osseointegrated implants, characterized by progressive alveolar bone destruction. The long non-coding RNA Negative Regulator of Interferon Response (IncRNA *NRIR*) is widely recognized as a biomarker for certain autoimmune diseases and participates in their pathogenesis. However, our previous studies revealed significant upregulation of *NRIR* in peri-implantitis, suggesting its potential role in peri-implantitis. In peri-implantitis lesions, there is often a substantial infiltration of M1 macrophages. Thus, this study investigated the regulatory role and underlying mechanisms of *NRIR* in macrophage polarization during peri-implantitis.

Methods: Transcriptome sequencing analysis revealed radical S-adenosyl methionine domain containing 2 (RSAD2) as an NRIR-interacting mRNA in macrophages. Using siRNA gene knockdown technology, we suppressed NRIR and RSAD2 expression in M1 macrophages derived from THP-1 cells. Subsequently, we employed RT-qPCR, Western blot, flow cytometry, and immunofluorescence staining to assess the levels of inflammatory cytokines and M1 macrophage-associated markers, aiming to elucidate the involvement of NRIR/RSAD2/NF-κB axis in macrophage polarization. Supernatants from NRIRknockdown macrophages were collected to prepare the culture medium for bone marrow mesenchymal stem cells (BMSCs). The expression of osteogenicrelated factors in BMSCs was evaluated through RT-qPCR, Western blot, Alkaline phosphatase (ALP) activity, and alizarin red S (ARS) staining. Furthermore, a rat peri-implantitis model was established, and the degree of peri-implant tissue inflammation and bone loss was assessed using micro-CT scanning and immunohistochemistry after treatment with various macrophage supernatants. **Results:** NRIR knockdown reduced RSAD2 expression and suppressed activation of the NF-kB pathway, consequently decreasing inflammatory cytokines and M1 macrophage-associated cytokine expression in THP-1 macrophages. Functionally, NRIR knockdown in macrophages promoted osteogenic differentiation of BMSCs. In vivo experiments showed that supernatants derived from NRIR-knockdown macrophages resulted in reduced inflammatory infiltration, diminished bone resorption, and increased expression of osteogenesis-related factors.

Discussion: This study demonstrates that *NRIR* functions as a pro-inflammatory modulator in peri-implantitis by activating M1 macrophages through the *RSAD2/* NF- κ B axis, providing novel insights into peri-implantitis pathogenesis that may inform future preventive and therapeutic strategies.

KEYWORDS

LncRNA NRIR, macrophage polarization, peri-implantitis, osteogenic differentiation, NF- κ B, RSAD2

1 Introduction

Peri-implantitis is a severe biological complication resulting from bacterial biofilm accumulation in peri-implant tissues, causing inflammation of peri-implant mucosa and subsequent progressive bone loss (1). Over the last 30 years, peri-implantitis has emerged as a significant clinical concern in dentistry (2). Research in osteoimmunology indicates that continuous crosstalk between cells of the monocyte/macrophage/osteoclast lineage and the mesenchymal stem cell-osteoblast lineage determines whether a durable prosthesis-implant interface is established or implant loosening occurs (3). Therefore, exploring interactions between macrophages and mesenchymal stem cells can elucidate the pathogenesis of peri-implantitis.

Macrophages undergo polarization in response to environmental stimuli, with M1 macrophages critically involved in the development of bacterial-induced inflammation, while M2 macrophages contribute to inflammation resolution and tissue repair (4, 5). A large population of M1 macrophages accumulates at sites of bone destruction in chronic osteolytic conditions such as arthritis and periodontitis (6). These macrophages produce substantial amounts of proinflammatory cytokines (TNF-α, IL-1, IL-12, IFN-γ), chemokines, and matrix metalloproteinases, inducing osteoclastogenesis, tissue erosion, and progressive bone destruction (7-10). Studies have shown a significant correlation between increased M1 macrophage expression and deeper periodontal probing depths (11). Notably, samples from peri-implantitis lesions exhibit markedly increased M1 macrophage populations (12). This phenomenon likely contributes significantly to the destructive inflammatory response and severe peri-implant osteolysis characteristic of advanced periimplantitis stages.

In recent years, long non-coding RNAs (lncRNAs) have attracted considerable scientific interest due to their abundance and potential regulatory roles in cellular, molecular, and pathophysiological processes. LncRNAs interact with DNA, RNA, or proteins, thereby regulating transcriptional, post-transcriptional, and translational outcomes (13, 14). Studies on lncRNA functions have suggested their potential as diagnostic/prognostic biomarkers and therapeutic targets in inflammatory diseases, including peri-implantitis and periodontitis (15, 16). LncRNA Negative Regulator of Interferon Response (*NRIR*), an interferon-stimulated gene, is widely considered

to play an essential role in the pathogenesis of autoimmune skin diseases, such as systemic sclerosis and systemic lupus erythematosus (17–19). However, few studies have reported the relationship between *NRIR*, macrophage polarization, and peri-implantitis. Further elucidation of these underlying mechanisms will enhance our understanding of peri-implantitis pathogenesis and facilitate the development of preventive and therapeutic approaches.

Our previous studies demonstrated significant upregulation of *NRIR* in peri-implantitis soft tissues (20). The current study further investigates the role of *NRIR* in peri-implantitis-associated macrophage polarization. Through RNA sequencing, we preliminarily identified *RSAD2* as a potential target for *NRIR*. Subsequent *in vitro* experiments revealed that *NRIR* regulates *RSAD2* expression, which in turn influences NF-KB activation and M1 macrophage polarization. Furthermore, supernatants derived from *NRIR*-knockdown macrophages upregulated osteogenic factor expression in bone marrow mesenchymal stem cells (BMSCs) and alleviated inflammation and bone loss in a rat peri-implantitis model. Collectively, this study provides novel insights into peri-implantitis pathogenesis and may inform future strategies for prevention and treatment.

2 Materials and methods

2.1 Cell culture and stimulation

The THP-1 human monocytic cell line was purchased from Biospecies (Guangdong, China). THP-1 cells were cultured in Roswell Park Memorial Institute 1640 (RPMI 1640, Procell, Wuhan, China) medium supplemented with 10% fetal bovine serum (FBS, PAN, Aidenbach, Germany) and 1% penicillin-streptomycin (Beyotime, Shanghai, China). To induce differentiation into M1 macrophages, THP-1 cells were stimulated with 200 ng/ml phorbol 12-myristate 13-acetate (PMA, Sigma, Shanghai, China) for 24 h to form adherent M0 macrophages, followed by treatment with 100 ng/ml LPS and 20 ng/ml IFN- γ for 48 h.

Human mesenchymal stem cells were obtained from Oricell (Guangzhou, China) and cultured in Minimum Essential Medium α (α -MEM, Procell, Wuhan, China) supplemented with 10% FBS and 1% penicillin-streptomycin.

All cell cultures were maintained in Esco CelMate carbon dioxide (CO₂) incubators (Esco, Singapore) at 37 °C under 5% CO₂ conditions to simulate physiological environments.

2.2 Cell transfection

Small interfering RNAs (siRNAs) specifically targeting *NRIR* and *RSAD2* were purchased from OBIO (Shanghai, China), with non-targeted siRNA used as negative control (NC). The siRNA and NC sequences are provided in Supplementary Table S1. Overexpression plasmids containing full-length RSAD2 and control plasmids were also acquired from OBIO (Shanghai, China); plasmid details are shown in Supplementary Figure S1.

For siRNA transfection, 5×10^5 THP-1 cells were seeded into six-well plates and cultured for 24 h, followed by incubation in Opti-MEMI Reduced Serum Medium (31985-070, Gibco, California, USA) for an additional 12 h. Subsequently, 100 pmol of siRNA was transfected into each well using 7.0 μ l CALNPTM RNAi reagent A and 2.0 μ l CALNPTM RNAi reagent B (D-Nano, Beijing, China).

For plasmid transfection, 5×10^5 THP-1 cells were seeded into six-well plates for 24 h. Upon reaching approximately 80% confluency, 3 µg of plasmid DNA was transfected per well with 4.8 µl Lipofect5000 reagent and 200 µl Trans buffer (BIOG, Changzhou, China).

2.3 RNA sequencing

Total RNA was isolated from M1 macrophages using TRIzol reagent (Sangon, Shanghai, China) following the manufacturer's instructions. RNA quality assessment, library preparation, sequencing, quality control, mapping reads to the reference genome, and differential gene expression analyses were performed by Novogene Co., Ltd (Beijing, China). For functional annotation, Gene Ontology (GO, http://www.geneontology.org/) and Kyoto Encyclopedia of Genes and Genomes (KEGG, http://www.genome.jp/kegg/) analyses were conducted to elucidate gene functions and relevant pathways associated with differentially expressed genes (DEGs). Gene Set Enrichment Analysis (GSEA) was further performed to identify key KEGG signaling pathways. R software (version 4.40) was utilized to visually represent data through principal component analysis (PCA), volcano plots, heatmaps, and pathway enrichment plots. The RNA-seq data were deposited in the NCBI Sequence Read Archive (SRA) (https://www.ncbi.nlm.nih.gov/sra) (BioProject ID: PRJNA1281584; BioSample accession numbers: SAMN49569226, SAMN49569227, SAMN49569228, SAMN49569229, SAMN49569230, and SAMN49569231).

2.4 Quantitative real-time polymerase chain reaction

Total RNA was extracted from THP-1 macrophages and BMSCs using the SteadyPure Rapid RNA Extraction Kit

(Accurate Biology, Hunan, China). RNA was reverse-transcribed into complementary DNA (cDNA) using the Evo M-MLV RT Mix Kit (Accurate Biology, Hunan, China). Subsequently, RT-qPCR was performed using SYBR® Green Premix Pro Taq HS RT-qPCR Kit (Accurate biology, Hunan, China), following the manufacturer's instructions. Relative gene expression levels were calculated using the $2^{-\Delta\Delta Ct}$ method as described by Livak et al. (21). Primers synthesized by Sangon Biotech (Shanghai, China) are listed in Supplementary Table S2.

2.5 Western blotting

Total proteins were extracted from THP-1 cells and BMSCs using a total protein extraction kit (Keygen Biotech, Jiangsu, China). Protein concentrations were quantified using a BCA assay Kit (Beyotime, Beijing, China). After centrifugation (12,000 × g, 4°C, 10 min), protein lysates were separated by 10% or 12.5% SDS-PAGE and transferred onto polyvinylidene fluoride (PVDF) membranes. Membranes were blocked with 5% skimmed milk in Tris-buffered saline containing Tween-20 (TBST) at room temperature for 2 h, then incubated overnight (4°C) with primary antibodies against RSAD2 (Proteintech, 28089-1-AP, 1:1000), CD86 (Huabio, ET1606-50, 1:1000), iNOS (Huabio, HA722031, 1:1000), phospho-p65 (CST, 3033 T, 1:1000), p65 (Proteintech, 10745-1-AP, 1:1000), phospho-IκB (Huabio, HA722770, 1:1000), IκB (Huabio, ET1603-6, 1:1000), Osteopontin (OPN, Proteintech, 80912-4-RR, 1:4000), osteocalcin (OCN, Bioss, bs-4917R, 1:1000), runt-related transcription factor-2 (RUNX2, Huabio, ET1612-47, 1:5000), and GAPDH (Affinity, AF7021, 1:1000). Subsequently, membranes were washed three times in TBST (10 min each) and incubated with HRP-conjugated secondary antibodies (Goat anti-Rabbit IgG, Proteintech, SA00001-2, 1:4000) at room temperature for 2 h. Protein bands were visualized using enhanced chemiluminescence reagent (Affinity, West Virginia, USA) and an iBright CL1000 imaging system (Thermo, MA, USA). Semi-quantitative analysis of protein expression was performed using ImageJ software (v1.8.0, NIH, MD, USA).

2.6 Flow cytometry

Following successful macrophage polarization, THP-1 cells were harvested and filtered to prepare single-cell suspensions. Fc receptor-mediated nonspecific binding was blocked using human Fc receptor blocking solution (TruStain FcXTM, BioLegend, 422301). Cells were washed three times, stained on ice with PE-conjugated anti-CD86 antibody (Biolegend, 374205) in staining buffer containing 1% FBS, and analyzed using a FACSMelody flow cytometer (BD). Data analysis was performed using FlowJo software (Tree Star).

2.7 Immunofluorescence staining

THP-1 cells were fixed in 4% paraformaldehyde (PFA) for 30 min, permeabilized with 0.5% Triton X-100 for 30 min at room

temperature (20°C), and blocked with 5% goat serum in phosphate-buffered saline (PBS) for 1.5 h (37°C). Subsequently, cells were incubated overnight (4°C) with primary antibodies against CD86 (Huabio, ET1606-50, 1:500) and iNOS (Huabio, HA722031, 1:100). After three washes with PBS, cells were incubated with fluorescent secondary antibodies for 1 h (37°C, in darkness). Cell nuclei were counterstained with 4′,6-diamidino-2-phenylindole (DAPI, Solarbio, Beijing, China). Stained cells were visualized using laser scanning confocal microscopy (BC43 SR, OXFORD, UK).

2.8 Macrophage supernatant preparation

M0 macrophages were transfected and subsequently polarized into M1 macrophages using LPS/IFN- γ for 48 h. Cells were then washed three times with PBS and cultured in serum-free medium for an additional 24 h. SNs were collected, centrifuged (300 × g, 10 min) to remove cellular debris, and filtered (0.22 μ m filter). A portion of SNs was combined 1:1 with osteogenic induction medium (Oricell, Guangzhou, China) for BMSC co-culture experiments, and the remainder was used directly for *in vivo* experiments.

2.9 Alkaline phosphatase activity and alizarin red S staining

BMSCs underwent osteogenic induction upon reaching 80% confluency. After 14 days, ALP activity was assessed using an ALP staining Kit (Beyotime, Beijing, China). Calcium mineralization was evaluated after 21 days by Alizarin Red S (ARS) staining (Oricell, Guangzhou, China). Chromogenic reactions were visualized using a stereomicroscope (SZN71, SOPTOP, China).

2.10 *In vivo* experiment

Thirty male Sprague-Dawley (SD) rats (8 weeks old) were obtained from the Animal Center of Southwest Medical University. All surgical procedures were approved by the Animal Ethics Committee of Southwest Medical University (SWMU20210414) and followed the ARRIVE (Animal Research: Reporting of *In Vivo* Experiments) guidelines.

Detailed surgical procedures were described in our previous studies (22). Briefly, unilateral maxillary first molars of SD rats were extracted under general anesthesia induced by 4% isoflurane inhalation. After a 4-week healing period, rats were anesthetized similarly, and local anesthesia (articaine with 1:100,000 epinephrine; Primacaine, France) was administered at the surgical site. Gingival incisions were made in the maxillary first molar region, and implant sockets were prepared using a reamer (1.6 mm diameter). Customized Ti-6AL-4V screw-type implants (2mm diameter, 3mm thread length, 1.5mm smooth neck) (22) were then inserted. Four weeks were allowed for osseointegration. Seven rats

were excluded after four weeks due to death (n = 3) or implant loosening (n = 4). The remaining rats were randomly allocated into four groups using a random number table: (a) control group (n = 5); (b) LPS group (n = 6); (c) si-NC-SN group (n = 6); and (d) si-NRIR-SN group (n = 6).

Different treatments were applied to each group. In the LPS group, LPS derived from P. gingivalis (1 mg/mL, 10 µL per injection) was injected into the gingival sulcus around implants every three days for two weeks to establish peri-implantitis (23). PBS replaced LPS injections in the control group. Considering rats lack the NRIR gene, direct knockdown via vectors (such as nanoparticle- or adenovirus-mediated siRNA transfer) was infeasible. Referring to prior studies (Tahmasebi et al., Ma et al.) (24-26), we chose macrophage-secreted supernatants (SN) as media to investigate NRIR's role in animal models. Rats in the si-NC-SN group received SN from M1 macrophages transfected with nontargeting siRNA, while those in the si-NRIR-SN group received SN from NRIR siRNA-transfected M1 macrophages. SN (200 µL) was injected into both buccal and lingual gingiva around implants every 3 days for 2 weeks. Rats were sacrificed four weeks post-injection, and tissues were harvested for analysis.

2.11 Micro-computed tomography

Maxillae were scanned using micro-CT (Inveon PET CT, Siemens, Germany) with the following parameters: spot size (50 μm), tube voltage (80 kVp), tube current (500 μA), and total rotation (360°). Three-dimensional (3D) reconstructions were analyzed using Mimics (version 21.0) software. Peri-implant bone loss was assessed by measuring the distance from the most coronal marginal bone position to the apical implant head at distal, mesial, buccal, and palatal locations. Bone mineral density (BMD), trabecular thickness (Tb.Th), bone volume fraction (BV/TV), trabecular separation (Tb.Sp), and trabecular number (Tb.N) were quantified according to the micro-CT analysis guidelines outlined by Huang et al. (27).

2.12 Immunohistochemical analysis

Maxillary alveolar bone specimens were fixed in 4% paraformaldehyde and decalcified for 6 weeks 10% ethylene diamine tetraacetic acid (EDTA, Solarbio, Beijing, China). Subsequently, specimens were sectioned into 4 μ m slices (proximal-distal direction), blocked with 5% BSA for 1h, and incubated with primary antibodies overnight (4°C) according to manufacturer protocols. Slices were then incubated with DAB chromogenic solution, counterstained with hematoxylin (3 min), and visualized under an Olympus BX51 microscope (Tokyo, Japan). Semi-quantitative analysis was conducted using ImageJ software (v1.8.0, NIH, MD, USA). Staining intensity was quantified by calculating average optical density (AOD) as the ratio of integrated optical density (IntDen) of positively stained regions to the area (AOD = IntDen/Area).

2.13 Statistical analysis

Statistical significance was assessed using two-tailed Student's ttest or one-way ANOVA. Where ANOVA showed significant differences, Student-Newman-Keuls q (SNK-q) *post-hoc* tests were performed to identify statistically significant pairwise differences. Variables not meeting normal distribution criteria were analyzed using the Kruskal–Wallis H test. Statistical analyses were performed using SPSS software (version 27.0, SPSS Inc., Chicago, USA). Quantitative data are presented as mean \pm standard deviation (SD). Differences were considered statistically significant at P < 0.05.

3 Results

3.1 LncRNA *NRIR* participates in M1 macrophage polarization in peri-implantitis

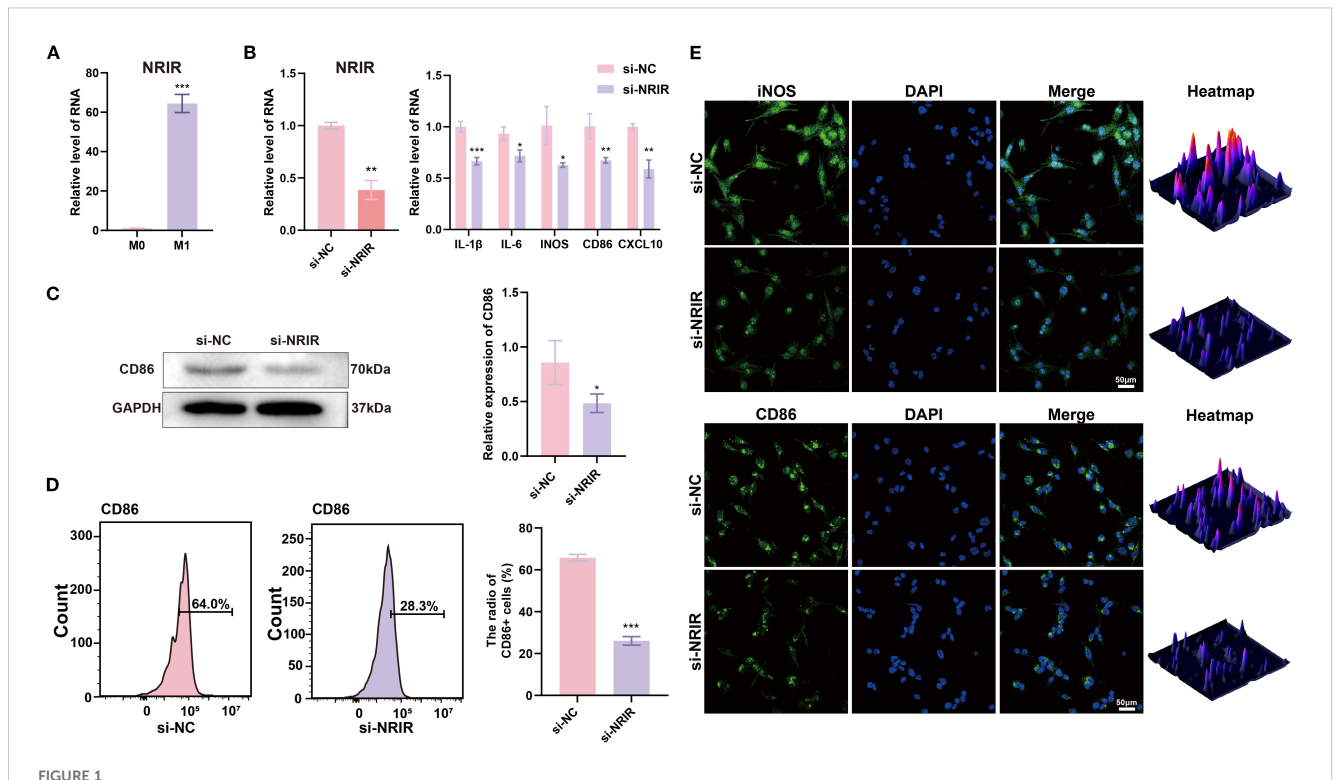
In our previous study, high-throughput transcriptome sequencing identified lncRNA *NRIR* in gingival tissues from perimplantitis patients. *NRIR* may critically contribute to peri-implant inflammation (20). Additionally, seven genes (*RSAD2*, *CMPK2*, *IFIT1*, *IFIT3*, *ISG15*, *BST2*, *and HLA-C*) were predicted as potential *NRIR* targets (20).

Since macrophages are pivotal immune cells in peri-implantitis, we hypothesized that *NRIR* might regulate macrophage polarization.

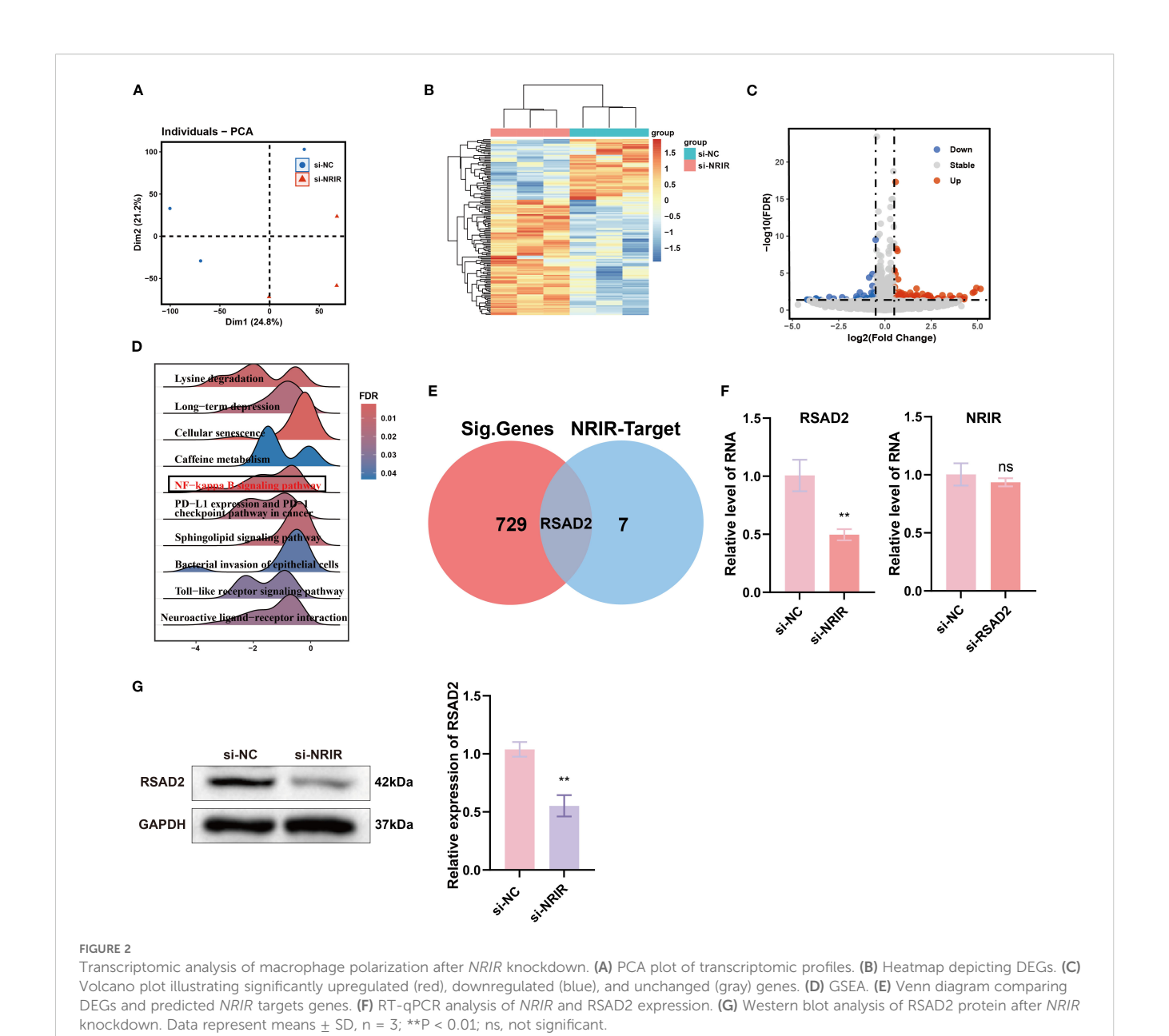
To test this hypothesis, we analyzed M1 macrophages and observed that *NRIR* was significantly upregulated (Figure 1A). Next, we used specific siRNA to silence *NRIR* and evaluated its influence on M1 macrophage activation. RT-qPCR results indicated significant downregulation of M1-associated genes (*IL-1β*, *IL-6*, *iNOS*, *CD86*, *and CXCL10*) following *NRIR* knockdown (Figure 1B). Western blotting demonstrated reduced CD86 protein expression in *NRIR*-knockdown macrophages (Figure 1C). Flow cytometry analysis revealed that *NRIR* knockdown significantly decreased M1 polarization, as indicated by CD86 (Figure 1D). Additionally, IF assays confirmed that *NRIR* silencing markedly inhibited expression of M1 macrophage polarization markers (iNOS, CD86) (Figure 1E).

3.2 *RSAD2* is a potential target of *NRIR* regulating macrophage polarization

To further explore the mechanisms underlying *NRIR*-mediated macrophage activation, we performed transcriptome microarray and bioinformatics analyses on M1 macrophages after *NRIR* knockdown. PCA and heatmap analyses demonstrated distinct transcriptomic profiles between control and *NRIR*-knockdown groups, indicating significant gene expression alterations (Figures 2A, B). Differential expression analysis identified 729 DEGs (357 downregulated, 372 upregulated), visualized by a volcano plot (Figure 2C). GSEA enrichment indicated general downregulation of the NF- κ B



LincRNA NRIR involvement in M1 macrophage polarization. (A) NRIR expression levels in M0 and M1 macrophages. (B) RT-qPCR analysis of NRIR and M1 polarization-related genes ($IL-1\beta$, IL-6, INOS, CD86, CXCL10) after NRIR knockdown. (C) Western blot analysis of CD86 protein expression after NRIR knockdown. (D) Flow cytometry evaluation of CD86-positive macrophages following NRIR knockdown. (E) IF staining of CD86 and iNOS after NRIR knockdown. Data represent means \pm SD, n = 3; *P < 0.05, **P < 0.01, ***P < 0.001; ns, not significant.



signaling pathway in *NRIR*-knockdown macrophages (Figure 2D). sign Additionally, intersection analysis between DEGs and predicted *NRIR* and targets identified *RSAD2* as the only overlapping gene (Figure 2E). RSA demininary characterization demonstrated that RSAD2 was downregulated following *NRIR* knockdown at both mRNA and protein levels, whereas *RSAD2* knockdown did not affect *NRIR* siler expression (Figures 2F, G). Thus, we strongly suspected *RSAD2* as a

3.3 *RSAD2* regulates M1 macrophage polarization

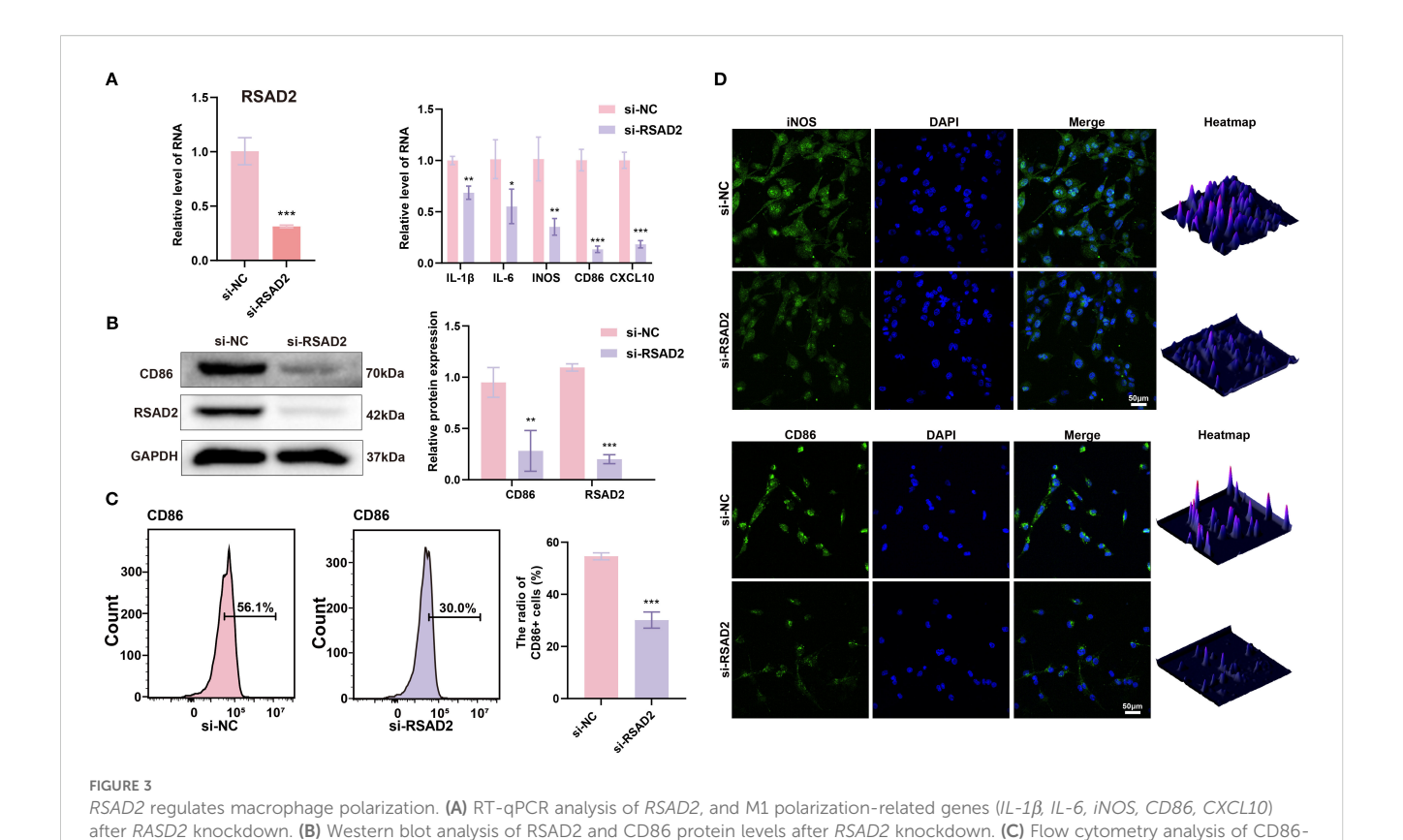
potential target of NRIR in macrophage polarization regulation.

To investigate the role of RSAD2 in M1 macrophages, RSAD2-knockdown macrophages were evaluated. At the genetic level, M1-associated genes (IL- 1β , IL-6, iNOS, CD86, and CXCL10) were

significantly downregulated (Figure 3A). At the protein level, *RSAD2*-knockdown macrophages showed reduced expression of RSAD2 and CD86 (Figure 3B). Flow cytometry results demonstrated that *RSAD2* knockdown markedly reduced M1 polarization (Figure 3C). Moreover, IF confirmed that *RSAD2* silencing effectively suppressed the expression of M1 macrophage polarization markers (iNOS, CD86) (Figure 3D).

3.4 LncRNA *NRIR* promotes M1 macrophage activation by enhancing RSAD2 gene expression

To confirm whether *NRIR* exerts its effects by regulating *RSAD2*, a rescue assay was conducted. Plasmids targeting *RSAD2* were transfected into THP-1 macrophages with confirmed *NRIR*



positive cells after RSAD2 knockdown. (D) IF staining of CD86 and iNOS after RSAD2 knockdown. Graphs represent means ± SD, n = 3; *P < 0.05,

knockdown to restore *RSAD2* expression. Results indicated that *RSAD2* overexpression reversed the reduced gene and protein expression associated with M1 macrophages caused by *NRIR* partices

3.5 Knockdown of IncRNA *NRIR* inhibits NF-κB signaling by downregulating *RSAD2* during macrophages polarization

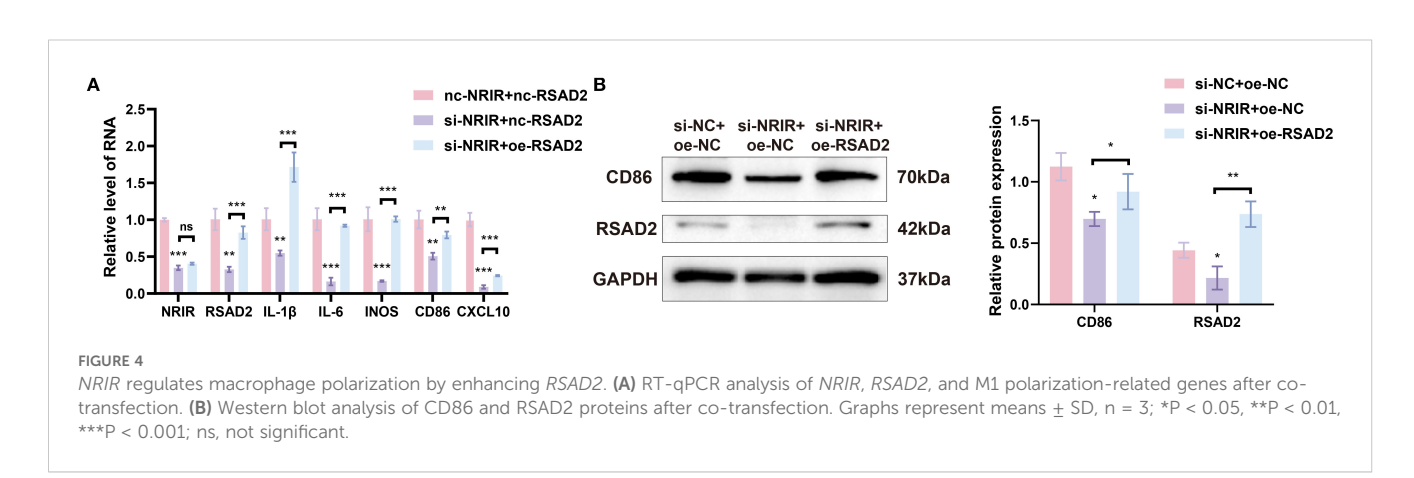
P < 0.01, *P < 0.001; ns, not significant.

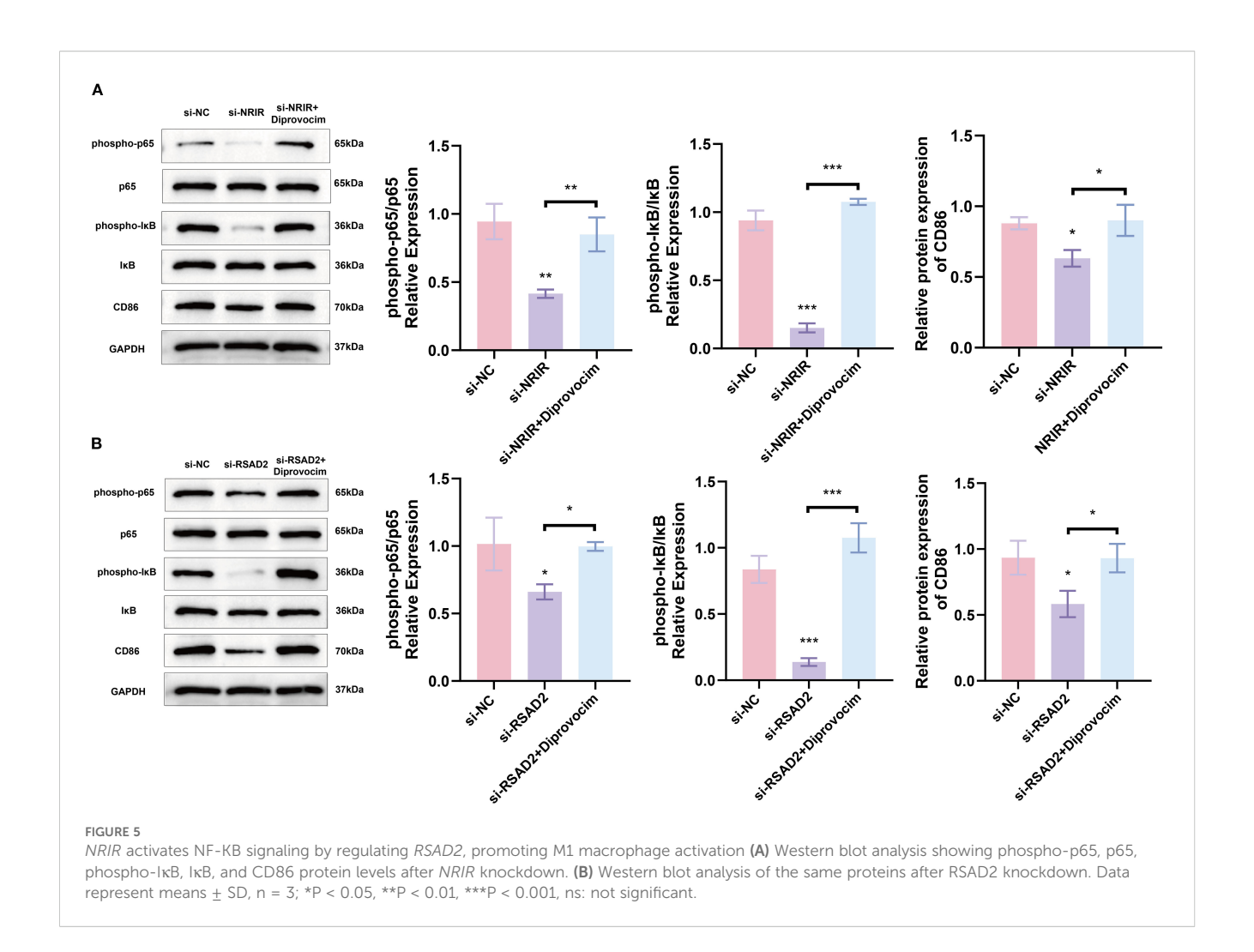
knockdown (Figures 4A, B).

We subsequently investigated signaling pathways regulated by NRIR during macrophage polarization. GSEA indicated that NRIR

knockdown inhibited the NF-κB signaling pathway (Figure 2D). The NF-κB pathway is essential for M1 macrophage activation, particularly in regulating inflammatory gene expression (28). Western blot analysis assessed phosphorylated forms of key factors, IκB and p65. Results showed that *NRIR* knockdown reduced phosphorylated IκB, phosphorylated p65, and CD86 levels in M1 macrophages. However, this reduction was reversed by treating cells with Diprovocim, a potent TLR1/TLR2 agonist that activates NF-κB signaling downstream (Figure 5A).

To confirm whether *NRIR* regulates NF-κB signaling via *RSAD2*, we evaluated *RSAD2*-knockdown macrophages. Protein levels of phosphorylated IκB, phosphorylated p65, and CD86





decreased in *RSAD2*-knockdown macrophages during M1 activation. These findings indicate that *NRIR* depletion suppresses NF-kB signaling by downregulating *RSAD2*, further attenuating M1 macrophage polarization (Figure 5B).

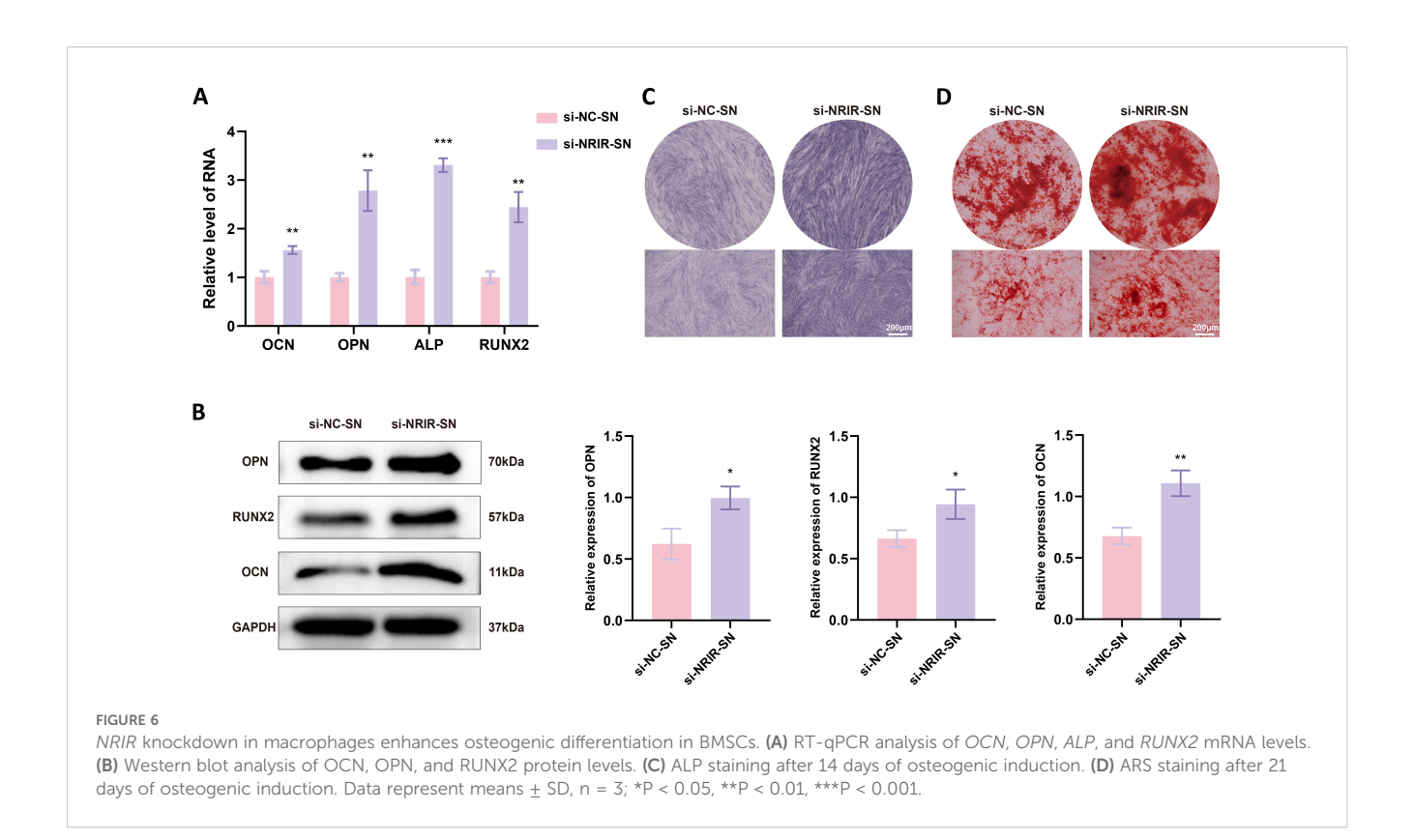
3.6 Macrophage with NRIR knockdown promote osteogenic differentiation of BMSCs in vitro

Chemokines and cytokines secreted by macrophages regulate MSC migration and differentiation for bone regeneration (29–31). To evaluate effects of factors secreted by NRIR-knockdown macrophages on BMSC osteogenic differentiation, conditioned medium from NRIR-knockdown M1 macrophages was used to culture BMSCs. RT-qPCR and Western blotting showed that NRIR-knockdown macrophage supernatants significantly increased expression of osteogenic differentiation markers (OCN, OPN, RUNX2) in BMSCs compared to control groups (Figures 6A, B). ALP staining demonstrated enhanced ALP expression in BMSCs cultured with NRIR-knockdown macrophage supernatants (Figure 6C). ARS staining showed that BMSCs cultured with

NRIR-knockdown macrophage supernatants formed more mineralized nodules (Figure 6D).

3.7 Supernatants from *NRIR*-knockdown M1 macrophages reduce inflammation and bone loss in a rat peri-implantitis model

Next, we explored the role of *NRIR* in peri-implantitis using a rat model. Clinical observations showed that supernatants from macrophages transfected with si-NC produced clinical manifestations similar to LPS-induced peri-implantitis. However, inflammation was significantly lower in rats treated with supernatants from macrophages transfected with si-*NRIR* (Figure 7A). Micro-CT revealed that bone loss in the si-NC-SN group and LPS group was comparable, whereas bone resorption was significantly lower in the si-*NRIR* group (Figure 7B). Bone morphometric analysis demonstrated significantly increased BMD, BV/TV, Tb.N, and Tb.Th and decreased Tb.Sp in the si-*NRIR*-SN group compared to the si-NC-SN group (Figure 7C). Additionally, histological analyses showed similar inflammatory infiltration and bone resorption in the LPS and si-NC-SN groups,



whereas the si-NRIR-SN group had reduced inflammatory cytokine expression (IL-1 β , IL-6, TNF- α) and elevated osteogenic marker expression (RUNX2, OPN, OCN) (Figures 7D, E). Together, NRIR knockdown modifies supernatant composition, reducing perimplant inflammation and bone loss.

4 Discussion

Over the past few decades, lncRNAs were considered transcriptional "junk" because they do not encode proteins (32). However, recent studies have demonstrated that lncRNAs play critical roles in the activation and function of differentially polarized macrophages in cancer, inflammation, and cardiovascular diseases (19, 33, 34). The present study identified lncRNA-NRIR, which regulated RSAD2 and was highly expressed during M1 macrophage activation. Using loss-of-function approaches, NRIR was determined to be a positive regulator of M1 macrophage activation in peri-implantitis. NRIR promotes NF-KB activation through RSAD2, reduces osteogenesis-related factors in BMSCs, and promotes inflammation-induced bone resorption in peri-implantitis (Figure 8). These findings suggest a novel regulatory pathway for M1 macrophage activation, providing new insights into peri-implantitis pathogenesis.

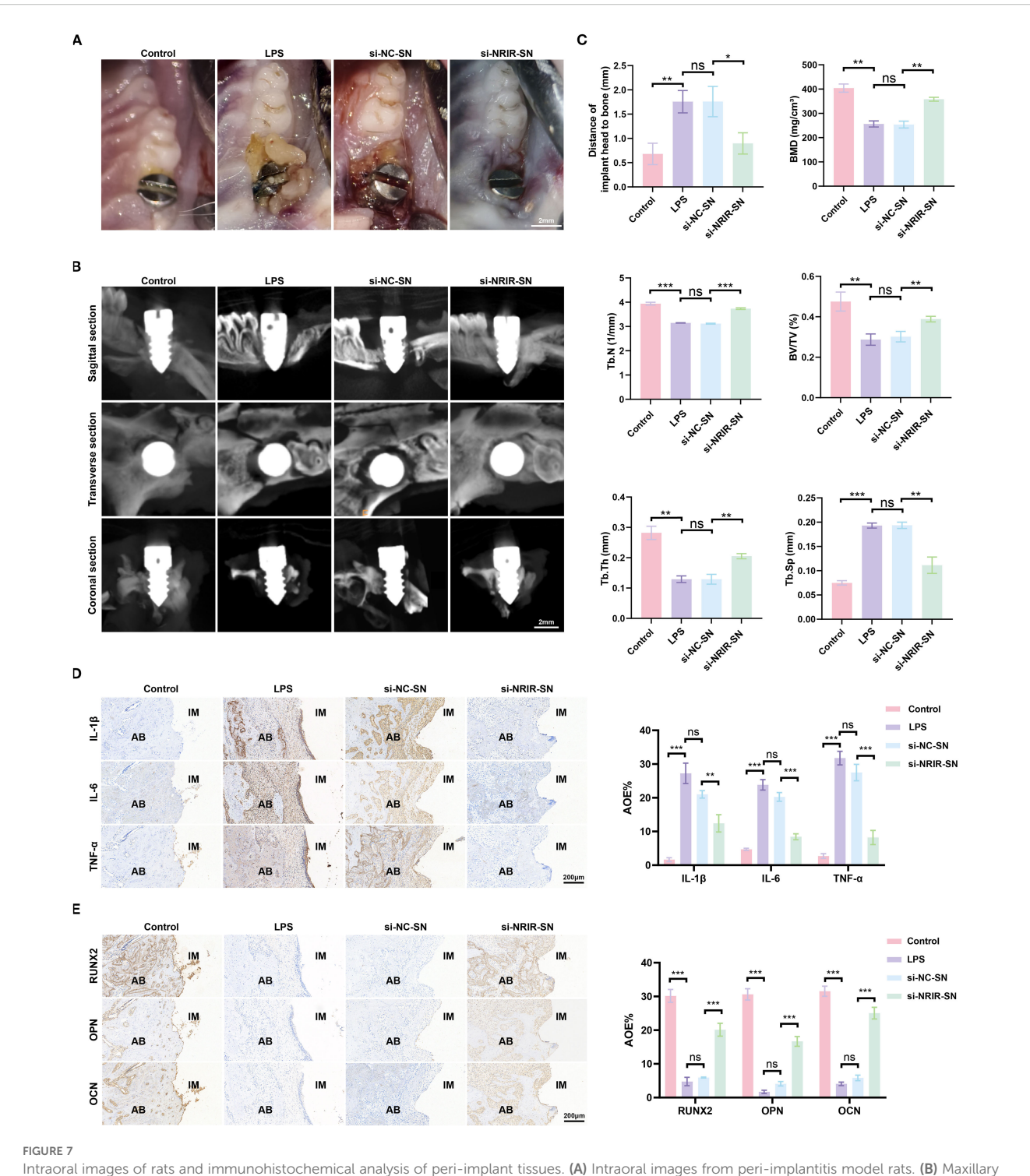
NRIR is located on chromosome 2p25.2 and is closely associated with the type I IFN pathway (35). Previous studies have identified NRIR as a potential biomarker for systemic lupus erythematosus (SLE), where it may contribute to disease progression (17–19). However, its roles and molecular mechanisms in other diseases,

especially macrophage-related conditions, remain poorly understood. A recent report indicated *NRIR* is strongly induced in macrophages during Mtb infection (36). In our study, *NRIR* was similarly induced in LPS/IFN-γ-stimulated M1 macrophages.

RSAD2 is an interferon-stimulated gene (ISG) encoding the protein viperin, known for antiviral activity (37). Emerging studies emphasize the critical roles of RSAD2/viperin in immunomodulation and mitochondrial metabolism (38–41). Although RSAD2 expression was significantly increased in polarized human THP-1 and mouse RAW264.7 macrophage models, its precise role in M1 macrophage activation remains unclear (42). Our study revealed that RSAD2/viperin participates in M1 macrophage activation. Moreover, based on previous high-throughput sequencing data and the findings of Cao et al., we verified NRIR regulates RSAD2, influencing macrophage polarization (20, 43).

As a pivotal inflammatory regulator, nuclear factor kappa-B (NF- κ B) promotes the transcription of pro-inflammatory cytokine genes (44). Previous studies confirmed that NF- κ B signaling regulates macrophage polarization (45–47). Transcriptome analysis from *NRIR*-knockdown M1 macrophages demonstrated significant down-regulation of NF- κ B signaling. Subsequent experiments provided strong evidence that *NRIR* activates NF- κ B signaling through *RSAD2*.

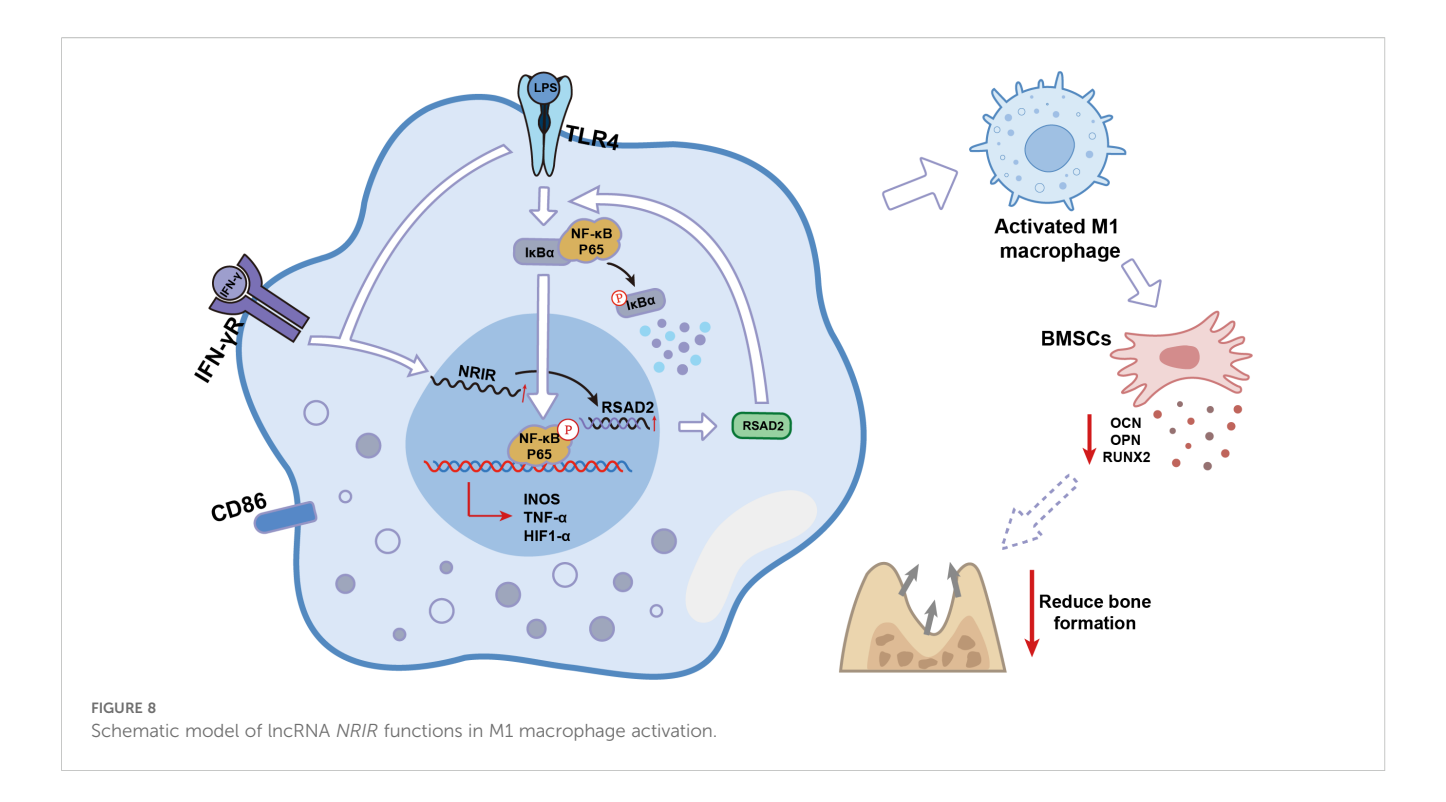
The immune and skeletal systems contribute to peri-implantitis by exchanging cytokines, transcription factors, and signaling receptors (48, 49). Macrophages, key immune cells, specifically regulate bone homeostasis. Conversely, BMSCs, major osteoblast progenitors, differentiate into osteoblasts under appropriate conditions, enhancing osteogenesis (50, 51). Pro-inflammatory



Intraoral images of rats and immunohistochemical analysis of peri-implant tissues. **(A)** Intraoral images from peri-implantitis model rats. **(B)** Maxillary Micro-CT images of each group. **(C)** Bone loss and bone morphometric parameters (BMD, Tb.N, BV/TV, Tb.Th, Tb.Sp) quantified in each group. **(D)** Representative IHC images and semi-quantitative analyses of IL-1 β , IL-6, and TNF- α in peri-implant tissues. **(E)** Representative IHC images and semi-quantitative analyses of RUNX2, OPN, and OCN in peri-implant tissues. AB, alveolar bone; IM, implant; AOD, average optical density. Data represent means \pm SD, n = 5; *P < 0.05, **P < 0.01, ***P < 0.001, ns, not significant.

M1 macrophages secrete various cytokines (TNF- α , IL-1, IL-12, IFN- γ), chemokines, and matrix metalloproteinases, promoting osteoclastogenesis, tissue erosion, and progressive bone destruction (7–10, 52). Based on this principle, supernatants derived from M1 macrophages were utilized to induce peri-

implantitis. The results showed that peri-implantitis induced by si-NC macrophage supernatant resulted in a degree of bone loss equivalent to that induced by LPS. Nevertheless, low TNF- α concentrations (20 ng/mL) promote favorable osteogenic outcomes (53). In our experiments, supernatants obtained from



NRIR-knockdown M1 macrophages enhanced the expression of osteogenic differentiation markers in BMSCs and alleviated inflammation and bone loss around implants *in vivo*. This beneficial effect may be attributed to alterations in cytokine concentrations that promote the differentiation of BMSCs into osteoblasts.

In clinical settings, how to effectively treat patients by targeting NRIR is an important consideration. In recent years, gene knockdown has been achieved through RNA interference technology induced by siRNA, opening new avenues for innovative treatments for various diseases (54). Although siRNA-based therapy holds significant promise, its clinical application requires addressing limitations related to targeted delivery, off-target effects, and immunogenicity (55). Several strategies are currently employed to overcome these challenges. Studies have shown that viral vectors, lipid nanoparticles, chemical modifications, or tri-GalNAc conjugates can precisely deliver oligonucleotides to target sites (56, 57). Replacing 2'-O-Me at specific nucleotide sites in the seed region effectively inhibits offtarget activity of siRNA (58, 59). Designing siRNA molecules with specific structural modifications can reduce immune activation (60-64). Thus, siRNA targeting NRIR represents a promising treatment strategy for peri-implantitis.

However, this study has several limitations. First, the THP-1 cell line used does not fully reflect the behavior of primary macrophages in peri-implantitis. Second, although the rat peri-implantitis model is ideal, it cannot completely replicate human peri-implantitis pathology. Given these limitations and shortcomings, future research should focus on primary human macrophages and further explore these findings through non-human primate models.

In summary, this study elucidates the NRIR/RSAD2/NF-κB pathway regulating M1 macrophage activation, suggesting

potential therapeutic targets for peri-implantitis prevention and treatment. Our findings provide clinically relevant theoretical insights into macrophage polarization regulation associated with peri-implantitis pathogenesis.

5 Conclusion

NRIR acts as a pro-inflammatory regulator in peri-implantitis. It activates the NF-κB signaling pathway by up-regulating *RSAD2*, promoting M1 macrophage activation, and consequently inhibits osteogenic differentiation in BMSCs. These findings provide novel insights into the pathogenesis of peri-implantitis.

Data availability statement

The data presented in the study are deposited in the NCBI Sequence Read Archive (SRA) repository (https://www.ncbi.nlm.nih.gov/sra), accession number SAMN49569226, SAMN49569227, SAMN49569228, SAMN49569229, SAMN49569230, and SAMN49569231, here: https://www.ncbi.nlm.nih.gov/sra/?term=PRJNA1281584.

Ethics statement

The animal study was approved by the Animal Ethics Committee of Southwest Medical University. The study was conducted in accordance with the local legislation and institutional requirements.

Author contributions

RZ: Conceptualization, Supervision, Writing – review & editing, Methodology, Writing – original draft. LW: Writing – review & editing, Methodology, Conceptualization. YZ: Methodology, Writing – review & editing, Formal Analysis. KX: Writing – review & editing, Methodology, Supervision. QL: Writing – review & editing, Methodology. KY: Conceptualization, Methodology, Writing – original draft, Writing – review & editing.

Funding

The author(s) declare financial support was received for the research and/or publication of this article. This work was supported by the Science and Technology Planning Project of Luzhou City (2024SYF130) and the Innovative Leader Talent Programme of the Affiliated Stomatological Hospital of Southwest Medical University (2024LJ04).

Conflict of interest

The authors declare that the research was conducted in the absence of any commercial or financial relationships that could be construed as a potential conflict of interest.

References

- 1. Berglundh T, Armitage G, Araujo MG, Avila-Ortiz G, Blanco J, Camargo PM, et al. Peri-implant diseases and conditions: consensus report of workgroup 4 of the 2017 world workshop on the classification of periodontal and peri-implant diseases and conditions. *J Clin Periodontol.* (2018) 45 Suppl 20:S286–s91. doi: 10.1111/jcpe.12957
- 2. Berglundh T, Mombelli A, Schwarz F, Derks J. Etiology, pathogenesis and treatment of peri-implantitis: A european perspective. *Periodontol.* (2000) 2024). doi: 10.1111/prd.12549
- 3. Goodman SB, Gibon E, Gallo J, Takagi M. Macrophage polarization and the osteoimmunology of periprosthetic osteolysis. Curr Osteoporos Rep. (2022) 20:43–52. doi: 10.1007/s11914-022-00720-3
- 4. Yu T, Zhao L, Huang X, Ma C, Wang Y, Zhang J, et al. Enhanced activity of the macrophage M1/M2 phenotypes and phenotypic switch to M1 in periodontal infection. *J Periodontol.* (2016) 87:1092–102. doi: 10.1902/jop.2016.160081
- Palevski D, Levin-Kotler LP, Kain D, Naftali-Shani N, Landa N, Ben-Mordechai T, et al. Loss of macrophage wnt secretion improves remodeling and function after myocardial infarction in mice. J Am Heart Assoc. (2017) 6(1):e004387. doi: 10.1161/jaha.116.004387
- 6. Li Y, Li X, Guo D, Meng L, Feng X, Zhang Y, et al. Immune dysregulation and macrophage polarization in peri-implantitis. *Front Bioeng Biotechnol.* (2024) 12:1291880. doi: 10.3389/fbioe.2024.1291880
- 7. Cutolo M, Campitiello R, Gotelli E, Soldano S. The role of M1/M2 macrophage polarization in rheumatoid arthritis synovitis. *Front Immunol.* (2022) 13:867260. doi: 10.3389/fimmu.2022.867260
- 8. Hu K, Shang Z, Yang X, Zhang Y, Cao L. Macrophage polarization and the regulation of bone immunity in bone homeostasis. *J Inflammation Res.* (2023) 16:3563–80. doi: 10.2147/jir.S423819
- 9. Zhang H, Cai D, Bai X. Macrophages regulate the progression of osteoarthritis. Osteoarthritis Cartilage. (2020) 28:555–61. doi: 10.1016/j.joca.2020.01.007
- 10. Sun X, Gao J, Meng X, Lu X, Zhang L, Chen R. Polarized macrophages in periodontitis: characteristics, function, and molecular signaling. *Front Immunol.* (2021) 12:763334. doi: 10.3389/fimmu.2021.763334

Generative AI statement

The author(s) declare that no Generative AI was used in the creation of this manuscript.

Any alternative text (alt text) provided alongside figures in this article has been generated by Frontiers with the support of artificial intelligence and reasonable efforts have been made to ensure accuracy, including review by the authors wherever possible. If you identify any issues, please contact us.

Publisher's note

All claims expressed in this article are solely those of the authors and do not necessarily represent those of their affiliated organizations, or those of the publisher, the editors and the reviewers. Any product that may be evaluated in this article, or claim that may be made by its manufacturer, is not guaranteed or endorsed by the publisher.

Supplementary material

The Supplementary Material for this article can be found online at: https://www.frontiersin.org/articles/10.3389/fimmu.2025.1650984/full#supplementary-material

- 11. Galarraga-Vinueza ME, Obreja K, Khoury C, Begic A, Ramanauskaite A, Sculean A, et al. Influence of macrophage polarization on the effectiveness of surgical therapy of peri-implantitis. *Int J Implant Dent.* (2021) 7:110. doi: 10.1186/s40729-021-00391-2
- 12. Fretwurst T, Garaicoa-Pazmino C, Nelson K, Giannobile WV, Squarize CH, Larsson L, et al. Characterization of macrophages infiltrating peri-implantitis lesions. *Clin Oral Implants Res.* (2020) 31:274–81. doi: 10.1111/clr.13568
- 13. Engreitz JM, Ollikainen N, Guttman M. Long non-coding rnas: spatial amplifiers that control nuclear structure and gene expression. *Nat Rev Mol Cell Biol.* (2016) 17:756–70. doi: 10.1038/nrm.2016.126
- 14. Yao ZT, Yang YM, Sun MM, He Y, Liao L, Chen KS, et al. New insights into the interplay between long non-coding rnas and rna-binding proteins in cancer. *Cancer Commun (Lond)*. (2022) 42:117–40. doi: 10.1002/cac2.12254
- 15. Liao K, Xu J, Yang W, You X, Zhong Q, Wang X. The research progress of lncrna involved in the regulation of inflammatory diseases. *Mol Immunol.* (2018) 101:182–8. doi: 10.1016/j.molimm.2018.05.030
- 16. Liu Y, Liu Q, Li Z, Acharya A, Chen D, Chen Z, et al. Long non-coding rna and mrna expression profiles in peri-implantitis vs periodontitis. *J Periodontal Res.* (2020) 55:342-53. doi: 10.1111/jre.12718
- 17. Shen M, Duan C, Xie C, Wang H, Li Z, Li B, et al. Identification of key interferon-stimulated genes for indicating the condition of patients with systemic lupus erythematosus. *Front Immunol.* (2022) 13:962393. doi: 10.3389/fimmu.2022.962393
- 18. Ma Q, Li L, Xing Y. Lncrna NRIR serves as a biomarker for systemic lupus erythematosus and participates in the disease progression. *Lupus*. (2024) 33:1538–46. doi: 10.1177/09612033241294032
- 19. Muntyanu A, Le M, Ridha Z, O'Brien E, Litvinov IV, Lefrançois P, et al. Novel role of long non-coding rnas in autoimmune cutaneous disease. *J Cell Commun Signal*. (2022) 16:487–504. doi: 10.1007/s12079-021-00639-x
- 20. Wang L, Zhao R, Xiao K, Zhou Y, Liu Q, Yu K. Long non-coding rna NRIR inhibits osteogenesis in peri-implantitis by promoting nlrp3 inflammasome-mediated macrophage pyroptosis. *Int Immunopharmacol.* (2025) 148:114180. doi: 10.1016/j.intimp.2025.114180

- 21. Livak KJ, Schmittgen TD. Analysis of relative gene expression data using real-time quantitative pcr and the 2(-delta delta C(T)) method. *Methods*. (2001) 25:402–8. doi: 10.1006/meth.2001.1262
- 22. Liu QQ, Wu WW, Yang J, Wang RB, Yuan LL, Peng PZ, et al. A gp130-targeting small molecule, Imt-28, reduces lps-induced bone resorption around implants in diabetic models by inhibiting il-6/gp130/jak2/stat3 signaling. *Mediators Inflammation*. (2023) 2023;9330439. doi: 10.1155/2023/9330439
- 23. Pirih FQ, Hiyari S, Leung HY, Barroso AD, Jorge AC, Perussolo J, et al. A murine model of lipopolysaccharide-induced peri-implant mucositis and peri-implantitis. *J Oral Implantol.* (2015) 41:e158–64. doi: 10.1563/aaid-joi-D-14-00068
- 24. Tahmasebi F, Asl ER, Faghihi F, Bolandi N, Barati S. Synergistic effects of olfactory ecto-mesenchymal stem cell supernatant and ellagic acid on demyelination and glial modulation in a chronic multiple sclerosis model. *Cell Mol Neurobiol.* (2025) 45:40. doi: 10.1007/s10571-025-01558-w
- 25. Tahmasebi F, Asl ER, Vahidinia Z, Faghihi F, Barati S. The comparative effects of bone marrow mesenchymal stem cells and supernatant transplantation on demyelination and inflammation in cuprizone model. *Mol Biol Rep.* (2024) 51:674. doi: 10.1007/s11033-024-09628-w
- 26. Ma SY, Zhao N, Cui L, Li Y, Zhang H, Wang J, et al. Therapeutic effects of human pluripotent stem cell-derived mesenchymal stem cells on a murine model of acute type-2-dominated airway inflammation. *Stem Cell Rev Rep.* (2022) 18:2939–51. doi: 10.1007/s12015-022-10389-x
- 27. Huang HL, Chen MY, Hsu JT, Li YF, Chang CH, Chen KT. Three-dimensional bone structure and bone mineral density evaluations of autogenous bone graft after sinus augmentation: A microcomputed tomography analysis. *Clin Oral Implants Res.* (2012) 23:1098–103. doi: 10.1111/j.1600-0501.2011.02273.x
- 28. Murray PJ. Macrophage polarization. Annu Rev Physiol. (2017) 79:541–66. doi: $10.1146/\mathrm{annurev}$ -physiol-022516-034339
- 29. O'Keefe RJ. Fibrinolysis as a target to enhance fracture healing. N Engl J Med. (2015) 373:1776–8. doi: 10.1056/NEJMcibr1510090
- 30. Kovach TK, Dighe AS, Lobo PI, Cui Q. Interactions between mscs and immune cells: implications for bone healing. *J Immunol Res.* (2015) 2015:752510. doi: 10.1155/2015/752510
- 31. Ono T, Takayanagi H. Osteoimmunology in bone fracture healing. Curr Osteoporos Rep. (2017) 15:367–75. doi: 10.1007/s11914-017-0381-0
- 32. Rafiee A, Riazi-Rad F, Havaskary M, Nuri F. Long noncoding rnas: regulation, function and cancer. *Biotechnol Genet Eng Rev.* (2018) 34:153–80. doi: 10.1080/02648725.2018.1471566
- 33. Meng Z, Zhang R, Wu X, Piao Z, Zhang M, Jin T. Lncrna haglros promotes breast cancer evolution through mir-135b-3p/col10a1 axis and exosome-mediated macrophage M2 polarization. *Cell Death Dis.* (2024) 15:633. doi: 10.1038/s41419-024-07020-x
- 34. Xue Y, Hu Y, Yu S, Zhu W, Liu L, Luo M, et al. The lncrna gas5 upregulates anxa2 to mediate the macrophage inflammatory response during atherosclerosis development. *Heliyon*. (2024) 10:e24103. doi: 10.1016/j.heliyon.2024.e24103
- 35. Mariotti B, Servaas NH, Rossato M, Tamassia N, Cassatella MA, Cossu M, et al. The long non-coding rna NRIR drives ifn-response in monocytes: implication for systemic sclerosis. *Front Immunol.* (2019) 10:100. doi: 10.3389/fimmu.2019.00100
- 36. Arumugam P, Singla M, Lodha R, Rao V. Identification and characterization of novel infection associated transcripts in macrophages. *RNA Biol.* (2021) 18:604–11. doi: 10.1080/15476286.2021.1989217
- 37. Fitzgerald KA. The interferon inducible gene: viperin. *J Interferon Cytokine Res.* (2011) 31:131–5. doi: 10.1089/jir.2010.0127
- 38. Xin Y, He Z, Mei Y, Li X, Zhao Z, Zhao M, et al. Interferon-A Regulates abnormally increased expression of rsad2 in th17 and tfh cells in systemic lupus erythematosus patients. *Eur J Immunol.* (2023) 53:e2350420. doi: 10.1002/eji.202350420
- 39. Qiu LQ, Cresswell P, Chin KC. Viperin is required for optimal th2 responses and T-cell receptor-mediated activation of nf-kappab and ap-1. *Blood*. (2009) 113:3520–9. doi: 10.1182/blood-2008-07-171942
- 40. Khantisitthiporn O, Shue B, Eyre NS, Nash CW, Turnbull L, Whitchurch CB, et al. Viperin interacts with pex19 to mediate peroxisomal augmentation of the innate antiviral response. *Life Sci Alliance*. (2021) 4(7):e20200091. doi: 10.26508/lsa.202000915
- 41. Seo JY, Yaneva R, Hinson ER, Cresswell P. Human cytomegalovirus directly induces the antiviral protein viperin to enhance infectivity. *Science*. (2011) 332:1093–7. doi: 10.1126/science.1202007
- 42. Li P, Hao Z, Wu J, Ma C, Xu Y, Li J, et al. Comparative proteomic analysis of polarized human thp-1 and mouse raw264.7 macrophages. *Front Immunol.* (2021) 12:700009. doi: 10.3389/fimmu.2021.700009

- 43. Cao H, Li D, Lu H, Sun J, Li H. Uncovering potential lncrnas and nearby mrnas in systemic lupus erythematosus from the gene expression omnibus dataset. *Epigenomics.* (2019) 11:1795–809. doi: 10.2217/epi-2019-0145
- 44. Guo Q, Jin Y, Chen X, Ye X, Shen X, Lin M, et al. Nf-Kb in biology and targeted therapy: new insights and translational implications. *Signal Transduct Target Ther.* (2024) 9:53. doi: 10.1038/s41392-024-01757-9
- 45. Zhuang L, Zong X, Yang Q, Fan Q, Tao R. Interleukin-34-nf-Kb signaling aggravates myocardial ischemic/reperfusion injury by facilitating macrophage recruitment and polarization. *EBioMedicine*. (2023) 95:104744. doi: 10.1016/jebiom.2023.104744
- 46. Wang S, Lu M, Wang W, Yu S, Yu R, Cai C, et al. Macrophage polarization modulated by nf-Kb in polylactide membranes-treated peritendinous adhesion. *Small.* (2022) 18:e2104112. doi: 10.1002/smll.202104112
- 47. Zhao H, Zhao H, Meng X, Zhao Z, Xie H, et al. Gbp5 exacerbates rosacea-like skin inflammation by skewing macrophage polarization towards M1 phenotype through the nf-Kb signalling pathway. *J Eur Acad Dermatol Venereol.* (2023) 37:796–809. doi: 10.1111/jdv.18725
- 48. Okamoto K, Nakashima T, Shinohara M, Negishi-Koga T, Komatsu N, Terashima A, et al. Osteoimmunology: the conceptual framework unifying the immune and skeletal systems. *Physiol Rev.* (2017) 97:1295–349. doi: 10.1152/physrev.00036.2016
- 49. Takayanagi H. Osteoimmunology: shared mechanisms and crosstalk between the immune and bone systems. *Nat Rev Immunol.* (2007) 7:292–304. doi: 10.1038/nri2062
- 50. Chen Z, Wu C, Gu W, Klein T, Crawford R, Xiao Y. Osteogenic differentiation of bone marrow mscs by B-tricalcium phosphate stimulating macrophages via bmp2 signalling pathway. *Biomaterials*. (2014) 35:1507–18. doi: 10.1016/j.biomaterials.2013.11.014
- 51. Pajarinen J, Lin T, Gibon E, Kohno Y, Maruyama M, Nathan K, et al. Mesenchymal stem cell-macrophage crosstalk and bone healing. *Biomaterials*. (2019) 196:80–9. doi: 10.1016/j.biomaterials.2017.12.025
- 52. Wan Z, Shin LY, Wang YF, Huang Z, Dong Y, Lee CW, et al. Role of skeletal macrophages in fracture repair: A systematic review. *BioMed Rep.* (2020) 13:53. doi: 10.3892/br.2020.1360
- 53. Mountziaris PM, Tzouanas SN, Mikos AG. Dose effect of tumor necrosis factoralpha on *in vitro* osteogenic differentiation of mesenchymal stem cells on biodegradable polymeric microfiber scaffolds. *Biomaterials*. (2010) 31:1666–75. doi: 10.1016/j.biomaterials.2009.11.058
- 54. Friedrich M, Aigner A. Therapeutic sirna: state-of-the-art and future perspectives. BioDrugs. (2022) 36:549–71. doi: 10.1007/s40259-022-00549-3
- 55. Nikam RR, Gore KR. Journey of sirna: clinical developments and targeted delivery. *Nucleic Acid Ther.* (2018) 28:209–24. doi: 10.1089/nat.2017.0715
- 56. Debacker AJ, Voutila J, Catley M, Blakey D, Habib N. Delivery of oligonucleotides to the liver with galnac: from research to registered therapeutic drug. *Mol Ther.* (2020) 28:1759–71. doi: 10.1016/j.ymthe.2020.06.015
- 57. Akinc A, Querbes W, De S, Qin J, Frank-Kamenetsky M, Jayaprakash KN, et al. Targeted delivery of rnai therapeutics with endogenous and exogenous ligand-based mechanisms. *Mol Ther.* (2010) 18:1357–64. doi: 10.1038/mt.2010.85
- 58. Kim M, Jeong M, Hur S, Cho Y, Park J, Jung H, et al. Engineered ionizable lipid nanoparticles for targeted delivery of rna therapeutics into different types of cells in the liver. *Sci Adv.* (2021) 7(9):eabf4398. doi: 10.1126/sciadv.abf4398
- 59. Chu R, Wang Y, Kong J, Pan T, Yang Y, He J. Lipid nanoparticles as the drug carrier for targeted therapy of hepatic disorders. *J Mater Chem B*. (2024) 12:4759–84. doi: 10.1039/d3tb02766j
- 60. Bumcrot D, Manoharan M, Koteliansky V, Sah DW. Rnai therapeutics: A potential new class of pharmaceutical drugs. *Nat Chem Biol.* (2006) 2:711–9. doi: 10.1038/nchembio839
- 61. Schwarz DS, Ding H, Kennington L, Moore JT, Schelter J, Burchard J, et al. Designing sirna that distinguish between genes that differ by a single nucleotide. *PloS Genet.* (2006) 2:e140. doi: 10.1371/journal.pgen.0020140
- 62. Hu B, Zhong L, Weng Y, Peng L, Huang Y, Zhao Y, et al. Therapeutic sirna: state of the art. Signal Transduct Target Ther. (2020) 5:101. doi: 10.1038/s41392-020-0207-x
- 63. Selvam C, Mutisya D, Prakash S, Ranganna K, Thilagavathi R. Therapeutic potential of chemically modified sirna: recent trends. *Chem Biol Drug Des.* (2017) 90:665–78. doi: 10.1111/cbdd.12993
- 64. Iribe H, Miyamoto K, Takahashi T, Kobayashi Y, Leo J, Aida M, et al. Chemical modification of the sirna seed region suppresses off-target effects by steric hindrance to base-pairing with targets. $ACS\ Omega.\ (2017)\ 2:2055-64.\ doi:\ 10.1021/\ acsomega.7b00291$